Engineering Geology 251 (2019) 81–92

Contents lists available at ScienceDirect

Engineering Geology

journal homepage: www.elsevier.com/locate/enggeo

Technical note

Quantitative analysis of debris-flow flexible barrier capacity from momentum and energy perspectives

D. Song[a,b], Gordon G.D. Zhou[a,b,*], Min Xu[c], C.E. Choi[d,e], S. Li[a], Y. Zheng[f]

[a] Key Laboratory of Mountain Hazards and Earth Surface Process, Institute of Mountain Hazards and Environment, Chinese Academy of Sciences (CAS), China
[b] University of Chinese Academy of Sciences, Beijing, China
[c] Geobrugg Chengdu Co., Ltd., Chengdu, China
[d] Department of Civil and Environmental Engineering, Hong Kong University of Science and Technology, Clear Water Bay, Kowloon, Hong Kong
[e] The HKUST Jockey Club Institute for Advanced Study, Hong Kong
[f] State Key Laboratory of Geomechanics and Geotechnical Engineering, Institute of Rock and Soil Mechanics, Chinese Academy of Sciences, China

ARTICLE INFO

Keywords:
Debris flow
Flexible barrier
Kinetic energy
Momentum flux
Debris-structure interaction

ABSTRACT

In-depth understanding of debris-structure interaction is hindered by a lack of physical data of debris flow impacting structures. This study reports a set of centrifuge experiments investigating the impact load exerted by debris flow on rigid and flexible barriers. A combination of high-speed imagery and load-displacement sensors enabled a comprehensive grasp of the impact details, including flow depth, velocity, impact pressure, bending moment, and cable force-elongation of flexible barrier. Test results reveal that the debris-structure interaction plays a major role in the energy dissipation and impact load reconstruction. The built-up of static load behind the barrier occurs simultaneously with the grow-up of impact force. As a result, the momentum flux of incoming flow is not merely a surrogate of the impact force. A quantitative analysis from the energy perspective has been conducted. Under the experimental conditions of this study, debris flow impact results in over 90% of debris energy dissipated through the internal and boundary shearing, leaving < 10% absorbed by the flexible barrier. Findings from the energy and momentum perspectives could facilitate the optimization of flexible barriers in mitigation of debris flow hazards.

1. Introduction

Estimation of debris flow impact load is one of the key procedures for design of engineering countermeasures, *i.e.*, rigid and flexible debris flow barriers, and is also a stringent way to comprehend the debris flow dynamic properties. Estimation of impact load on rigid barrier is on the basis of "momentum approach" (or "force approach"; Kwan, 2012; Wendeler et al., 2018). Theoretically, the momentum flux $\rho v^2 hw$, in the same dimension with force, is the upper limit of the dynamic load exerted on structures, where ρ is debris flow bulk density, v is flow velocity, and hw is impact area with height h and width w.

Debris-flow flexible barrier originates from the rockfall flexible barrier (Kwan et al., 2014; Duffy and DeNatale, 1996), which dissipates the kinetic energy of rock block mainly through the structural components of flexible barrier. Therefore, the precedent design of debris-flow flexible barrier was energy-based (Wendeler, 2008; Kwan and Cheung, 2012; Huo et al., 2017). In the "energy approach" recommended by Kwan and Cheung (2012), the calculation of energy transferred to the barrier is based on the idealized deposition mechanisms (*i.e.* pile-up and run-up mechanisms) and is limited to the specific conditions for their use. Since energy loss due to compression of the deposited debris mass has not been included in the calculation. This "energy approach" could result in a conservative estimate of impact energy (Kwan and Cheung, 2012). Moreover, the "energy approach" fails in detailing the internal structural forces of a flexible barrier, *e.g.*, the pressure distribution and cable force along barrier height. The continuous and distributed loading characteristics of debris flow completely differs from the pattern of rockfall impact. Thus, the flexible barrier structural integrity and foundation capacity cannot be directly evaluated using the "energy approach". As a result, design of debris-flow flexible barrier is oriented towards the "momentum approach" (WSL, 2009; Kwan and Cheung, 2012; Volkwein, 2014; Wendeler et al., 2018).

Currently, there lacks comprehensive analysis of debris-structure interaction due to the poor temporal practicability, complex flow

* Corresponding author at: Key Laboratory of Mountain Hazards and Earth Surface Process, Institute of Mountain Hazards and Environment, Chinese Academy of Sciences (CAS), China.
E-mail addresses: drsong@imde.ac.cn (D. Song), gordon@imde.ac.cn (G.G.D. Zhou), min.xu@geobrugg.com (M. Xu), ceclarence@ust.hk (C.E. Choi), lishuai@imde.ac.cn (S. Li), yzheng@whrsm.ac.cn (Y. Zheng).

https://doi.org/10.1016/j.enggeo.2019.02.010
Received 6 July 2018; Received in revised form 13 December 2018; Accepted 4 February 2019
Available online 07 February 2019
0013-7952/

Table 1
Relevant scaling laws (Schofield, 1980; Ng et al., 2016a).

Parameter	Dimension	Scaling law (model/prototype)
Gravity	L/T^2	$N = 22.4$
Length	L	$1/N$
Velocity	L/T	1
Inertial time	T	$1/N$
Force (momentum flux)	ML/T^2	$1/N^2$
Energy	ML^2/T^2	$1/N^3$

composition, and boundary conditions of natural events (Berger et al., 2011; Wei et al., 2017; Cui et al., 2017; Zhang, 1993), as well as the incomplete measurements on debris-resisting structures (Wendeler et al., 2007). The lack of direct measurements of the force and displacement in the flexible barrier system hinders the direct evaluation of debris-flow flexible barrier based on its rated energy capacity. Furthermore, quantification of the energy dissipated by the flexible barrier itself could reveal the mechanisms of debris-structure interaction and enhance the design of debris-resisting structures. By conducting a series of small-scale flume tests with slope inclination of 30°, Huo et al. (2017) reported that the ratio of kinetic energy dissipated within debris flow to the total kinetic energy is generally low, and the energy absorption efficiency by flexible barrier is approximately 64%. Note the energy absorption efficiency in Huo et al. (2017) was based on the analytical method proposed by Sun and Law (2015); also see Kwan and Cheung, 2012), assuming a steady state of debris flow process which is inconsistent with the inherent unsteady nature of mass-movement processes (Iverson, 2015). Using a numerical model calibrated by the large-scale filed test of debris flow impacting flexible barrier (the Veltheim field test with slope inclination of 30°, WSL, 2011), Kwan et al. (2018) found that only 6% of debris total energy (kinetic + potential energy) was transferred to the flexible barrier. While using the same software and by varying the slope inclination from 0° to 30°, Cheung et al. (2018) reported the energy absorption ratio to the total energy (kinetic + potential energy) ranging from 7% to 30%. It is thus imperative to investigate the energy dissipation mechanism based on reliable physical data.

This technical note takes advantage of a set of centrifuge simulation to scrutinize the debris flow impact from both momentum and energy perspectives. The total energy of debris flow and the rated energy capacity of a flexible barrier are compared to quantitatively evaluate the "energy approach" for debris-flow flexible barrier. The consideration of debris-structure interaction in enhancing the energy dissipation within debris flow and in estimating the debris flow impact force is highlighted.

2. Centrifuge modelling of impact on rigid and flexible barriers

2.1. Scaling

Centrifuge modelling ensures that the stress states in the prototype can be reasonably replicated by raising the field of gravity in a model (Schofield, 1980). Debris flows approach downstream a slope under the traction of gravitational field. Based on the conservation of energy, the flow inertia is characterized with a velocity scale of $v = (gl)^{1/2}$, where g is acceleration of gravity and l is length scale of the flow. In centrifuge simulation, the acceleration of gravity is elevated N (= 22.4) times and linear dimensions (*e.g.,* l, flow depth h, and width w) are scaled down N times, leading to a scale factor of unity of velocity (Song et al., 2018a). The momentum flux ($\rho v^2 hw$) passing through a specific cross section has the same dimension with that of debris impact force and is scaled with $1/N^2$. The energy and work done by debris-structure interaction have a factor of $1/N^3$ (Table 1). Details of scaling laws can be found in Ng et al. (2016a) and Song et al. (2018a).

2.2. Test setup and instrumentation

Fig. 1a presents a schematic of the debris flow impact model within a model container. The Perspex window of the model container allows for recording the impact kinematics using high-speed camera (Fig. 1b). Resolution of the high-speed camera is 1300 × 1600 pixels, which is fine enough for analyzing the flow depth and velocity using Particle Image Velocimetry (PIV). A slope with 25° inclination from the horizontal level was installed within the model container. A storage container (0.03 m^3) was used to continuously supply debris unto the upstream end of the slope. The release door was hinged at the bottom of the storage container. Once reached the targeted g-level (22.4 g), the bottom door could be triggered by a hydraulic actuator.

A steel plate was fixed at right angle to the slope to form a cantilever rigid barrier (Fig. 1a & c). This rigid barrier is equivalent to a prototype reinforced concrete wall 4.5 m in height, 5.2 m in width, and 0.9 m in thickness. To measure the induced bending moment along the barrier height, 15 sets of Wheatstone full bridge with semiconductor strain gauges were installed. Five dynamic load cells were inserted in the rigid barrier with their face flush with the barrier surface to measure the pressure distribution and the total impact force *via* integration. In the course of frontal impact of debris flow, the impact pressure gradient varies drastically at the lower portion of the barrier. The lower portion of rigid barrier was more densely instrumented than the upper portion (Song et al., 2017).

One rigid post, four steel strand horizontal cables with an impermeable membrane formed the face of a simplified flexible barrier system at the partition front (Fig. 1c). The other end of the horizontal cables went through a partition and were connected to individual spring mechanism (Fig. 1d). To replicate the loading characteristics of a prototype debris-flow flexible barrier, the spring mechanism consists of one relaxed and one preloaded compression springs in series. The load-displacement response is simplified as a bi-linear behavior with a stiffer initial stage and a softer second stage. Load cells and laser sensors were positioned along each horizontal cable to record the induced loads and cable displacement, respectively. Typical dynamic loading response of the spring mechanism is shown in Fig. 3c. Due to the inertial effect of the spring and cable, the load-displacement response is rate-dependent, *i.e.*, the loading (dynamic) response is slightly higher than the unloading (less dynamic) response. From the energy perspective, the model flexible barrier is equivalent to a prototype 1000 kJ debris flow barrier. Details for the model barrier can be found in Song et al. (2018b) and Ng et al. (2016a).

2.3. Two-phase debris flow materials and program

To reveal the fundamental impact mechanisms, simplified two-phase flows, instead of real debris flow materials, were adopted. The ideal two-phase flows of this study consists of uniform silica sand and pure viscous fluid (0.5 Pas in prototype). Leighton Buzzard fraction C sand was adopted as the solid phase and is characterized uniform and about 0.6 mm in diameter. The internal friction angle of this silica sand is measured as 31°. The viscous fluid represented the water-fine grain slurry which flows among the voids of granular material.

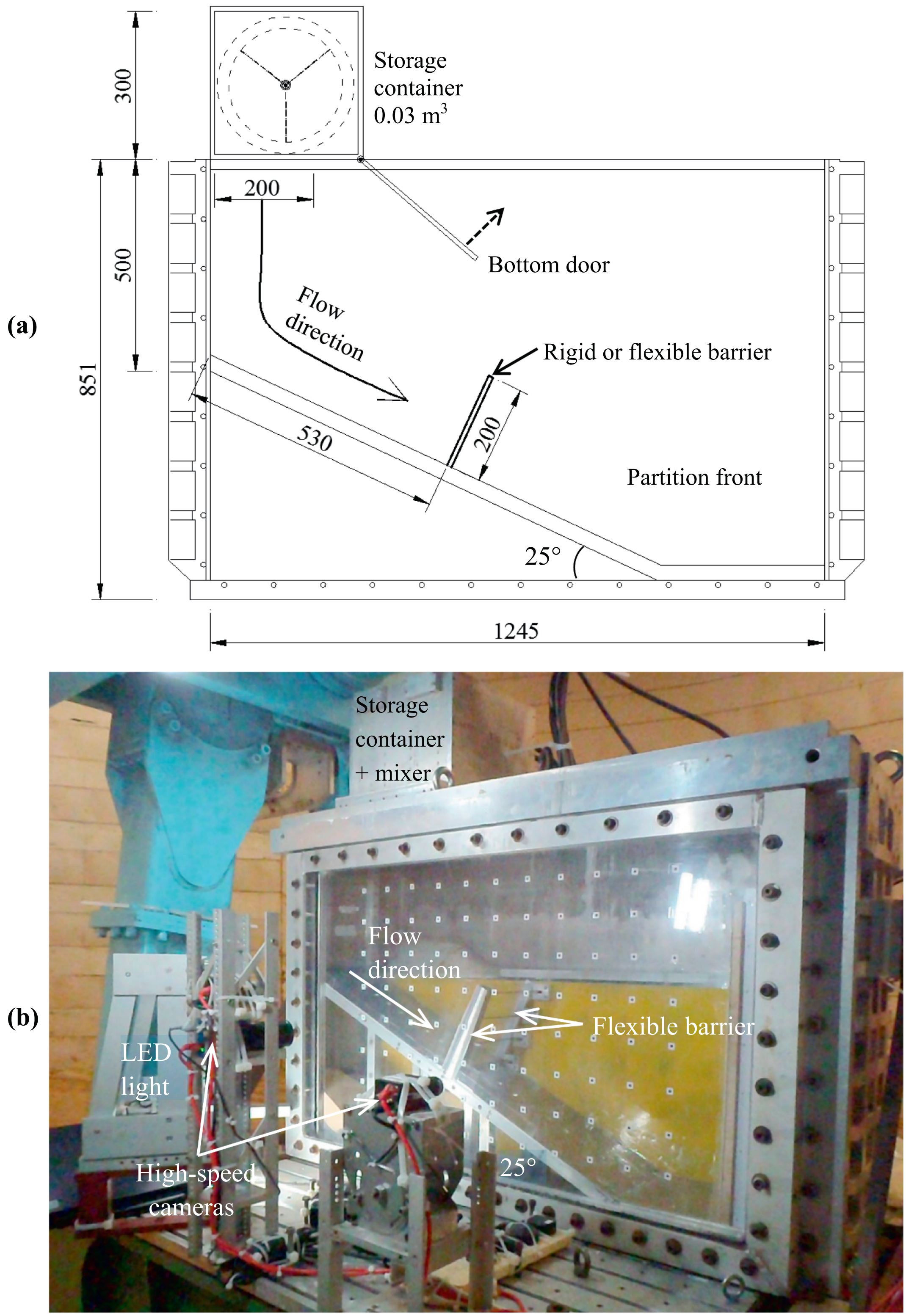

Fig. 1. (a) Schematic of the model setup in front of the partition; (b) side view of model setup in front of the partition; (c) front face of rigid barrier and instrumentation; and (d) oblique view of flexible barrier setup at the back of partition.

Before the debris flow impact tests, free-flow calibration tests without installation of a barrier were conducted to characterize the flow velocity and depth hydrograph using the high-speed camera. Impact tests on both rigid and flexible barriers were then performed. The solid fraction was varied as 0.2, 0.4, and 0.5 to cover a wide spectrum of debris flows (Table 3). One debris avalanche impact was also modelled using dry sand to cover the flow regime where grain-contact stress fully dominates over the viscous effect of interstitial air (Iverson et al., 2004).

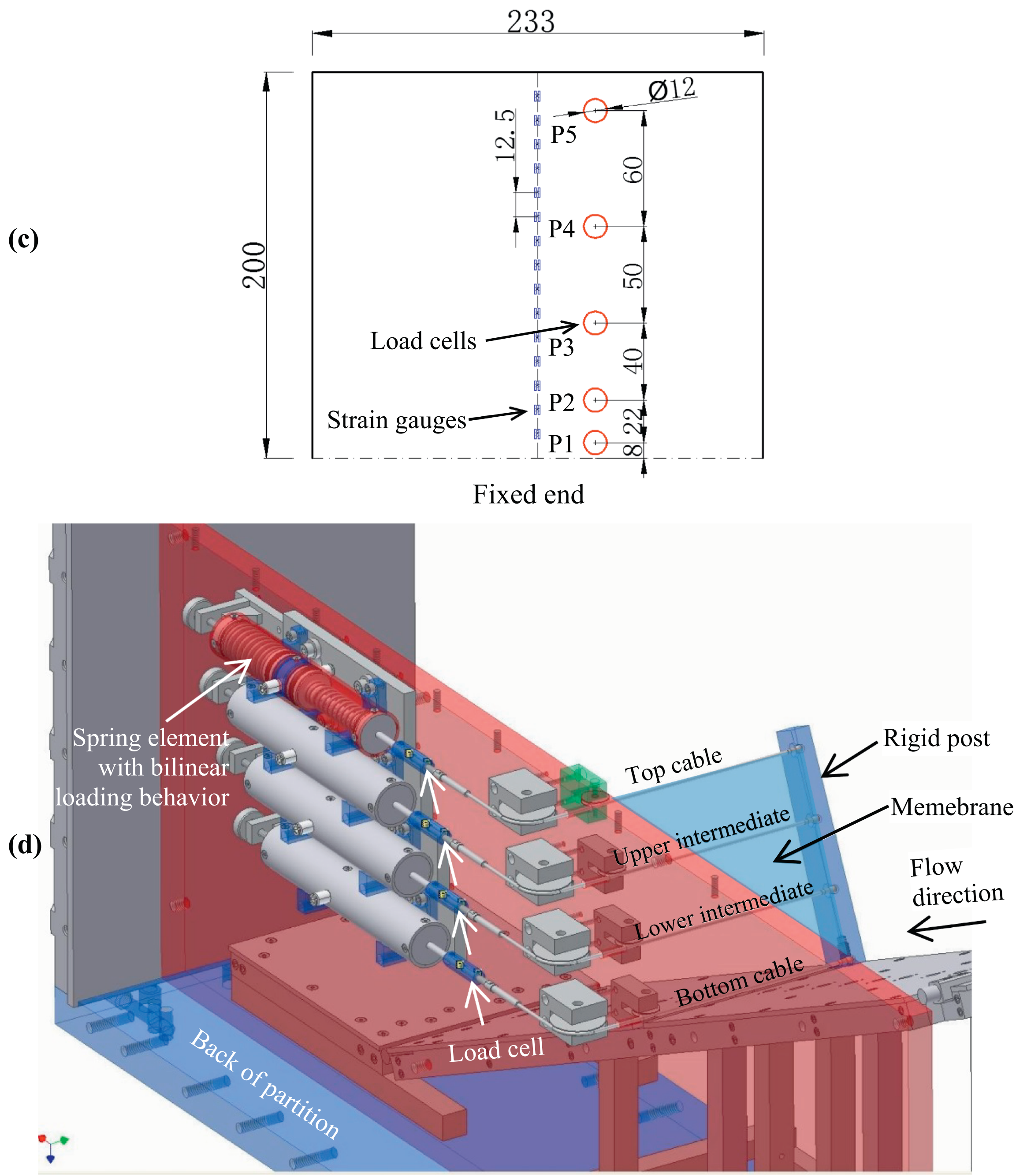

Fig. 1. (*continued*)

3. Results and interpretation

3.1. Dynamic response of flexible and rigid barriers

Fig. 2a shows a typical measured impact pressure time histories of the 50%-solid-fraction flow impacting rigid barrier. Along the barrier height, the sensors at the barrier base (P1 and P2) detected the maximum pressure which is characterized as a sharp impulse. After the initial impulse, the impact pressure experienced a rapid drop, followed by a much milder attenuation and eventually static condition (Song et al., 2017). The sensors at the upper portion of barrier (P3 – P5) did not detect the impact pressure until the two-phase flow ran up to the specific height. The pressure distribution forms the basis of derivation of total impact force through integration of pressure along the barrier height (see the blue continuous lines in Figs. 4b-7b). For the 50%-solid-fraction flow, the peak impact force occurred at $t = 0.9$ s when the

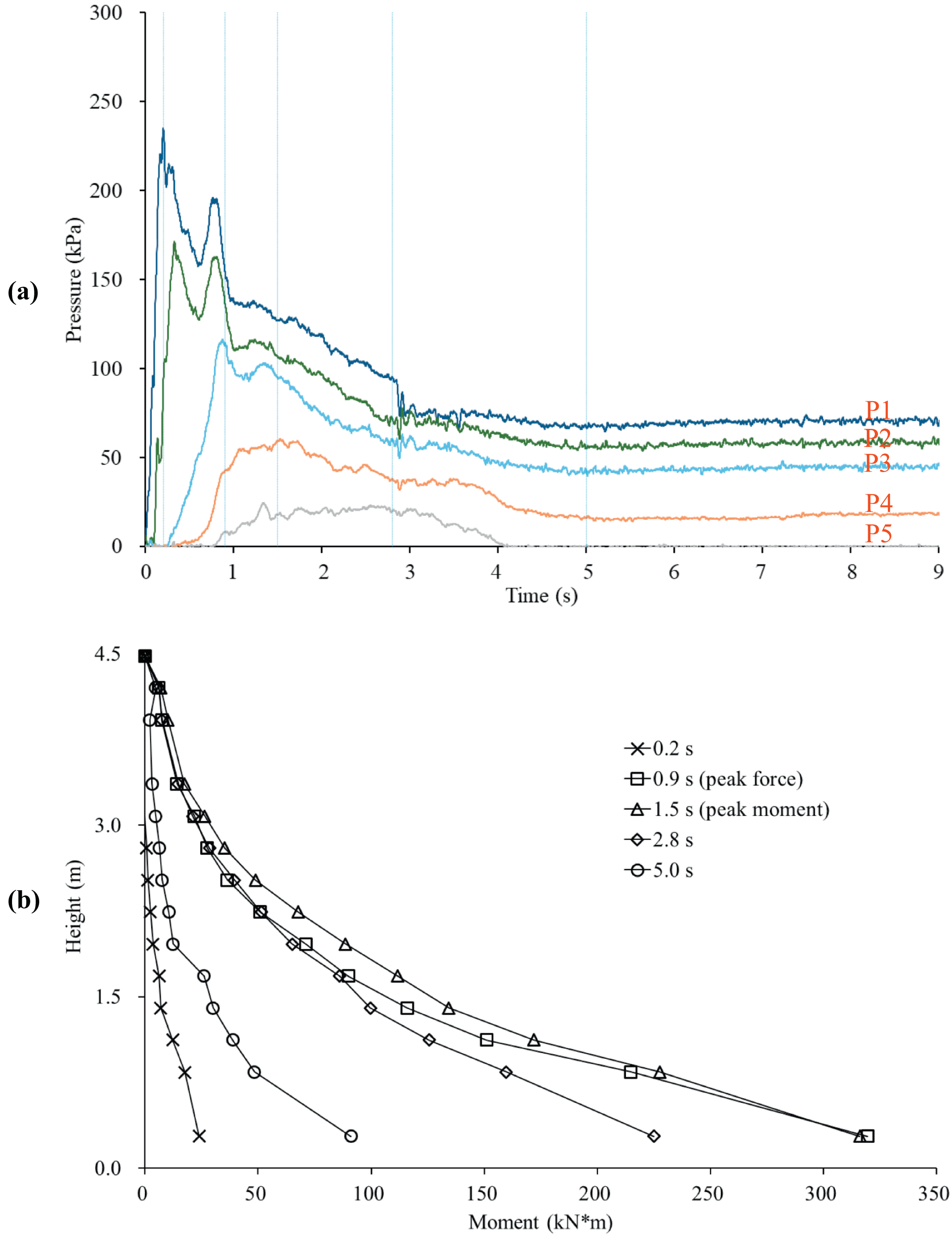

Fig. 2. Measured (a) impact pressure time history; and (b) bending moment profiles of rigid barrier impact by debris flow with 50% solid fraction.

impact pressure at P1 and P2 had already passed their peaks (Fig. 6b). The recorded bending moment distribution along the barrier height is nonlinear with the maximum developing at the base of barrier (Fig. 2b). As the run-up process proceeded, the impact force acting point shifted upwards. The peak bending moment occurred at $t = 1.5$ s when the total impact force had already passed its peak ($t = 0.9$ s).

The cable elongation of flexible barrier was recorded in synchronization with the axial cable load. Fig. 3a shows the typical cable elongation of the 50%-solid-fraction flow for the bottom, lower intermediate, upper intermediate, and top cables. The greatest elongation, 1.3 m in prototype, occurred in the lower intermediate cable but is close with the measurement in bottom cable. With the increase of barrier

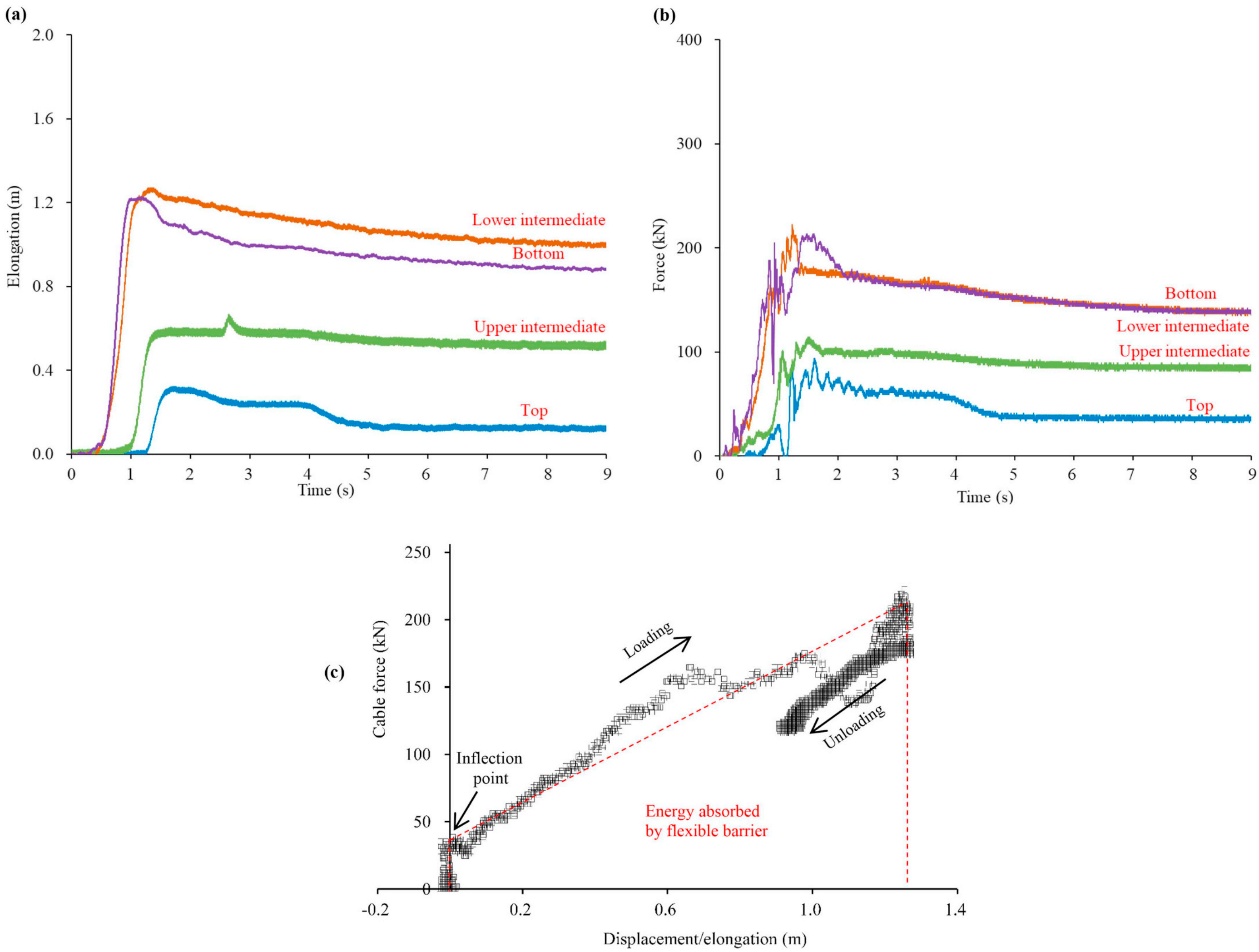

Fig. 3. (a) Cable elongation time history of test with 50% solid fraction; (b) measured cable force time history for with 50% solid fraction; (c) loading and unloading path of lower intermediate cable.

Table 2
Degree of cable utilization of flexible barrier.

Solid fraction (%)	Cable location	Maximum cable force (kN)	Degree of cable utilization (%, 350 kN as reference)
20	Top	81	23
	Upper intermediate	122	35
	Lower intermediate	288	82
	Bottom	297	85
40	Top	70	20
	Upper intermediate	121	35
	Lower intermediate	216	62
	Bottom	221	63
50	Top	94	27
	Upper intermediate	114	33
	Lower intermediate	222	63
	Bottom	213	61
Dry	Top	14	4
	Upper intermediate	25	7
	Lower intermediate	63	18
	Bottom	155	44

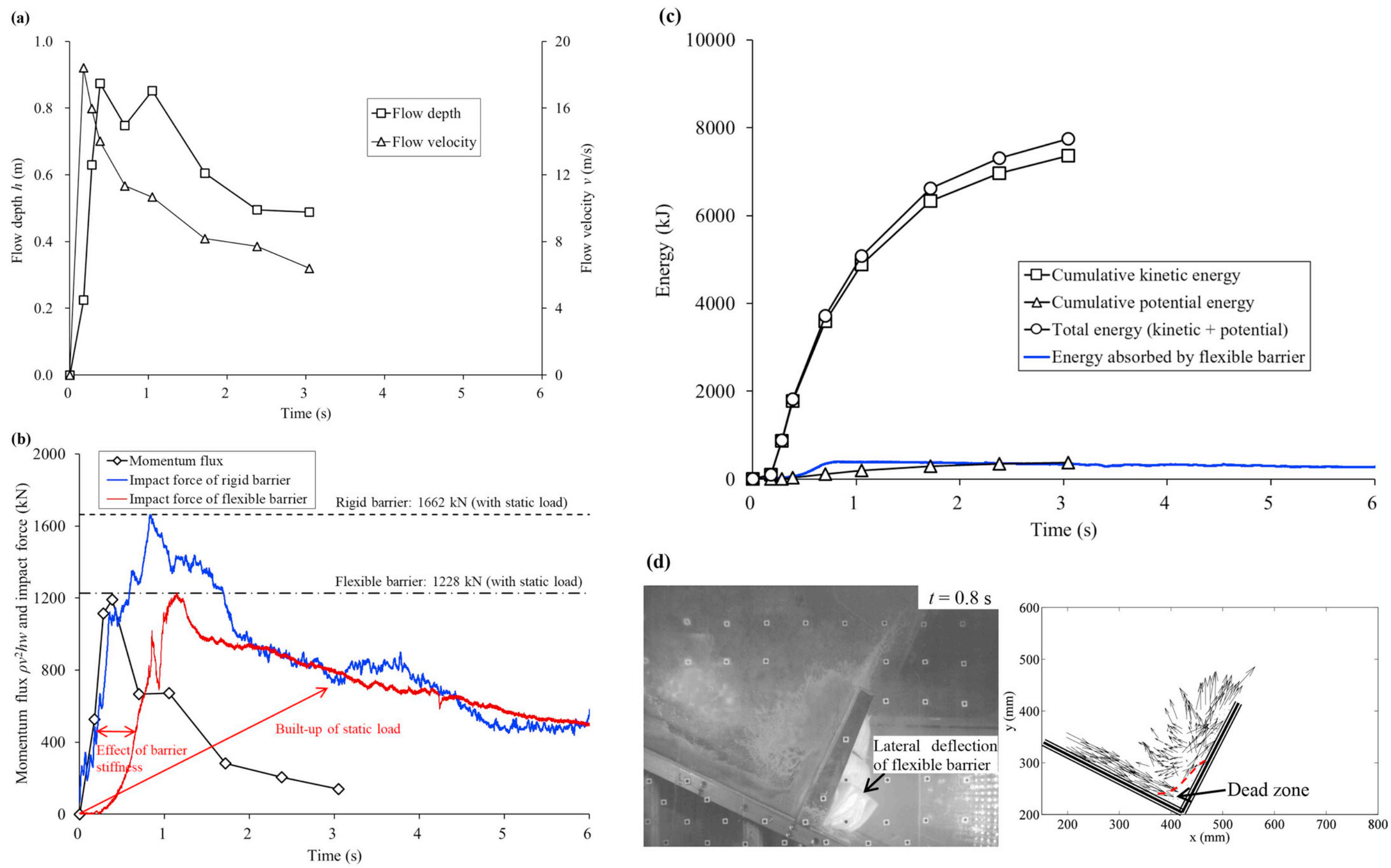

Fig. 4. Time histories of debris flow with 20% solid fraction (a) flow depth and velocity; (b) momentum flux and impact force; (c) debris energy and energy stored by flexible barrier; and (d) observed static load (dead zone revealed by PIV analysis) at the time instant when maximum energy is stored by flexible barrier.

height, the elongation in the top and upper intermediate cables drop drastically. The bottom and lower intermediate cables picked up loading right after the debris reaches the barrier base. Whereas the upper intermediate and top cables do not detect any loading until the debris reached the upper part of flexible barrier (Fig. 3b, Song et al., 2018b). Table 2 summarizes the maximum cable forces of each impact test. Since the centrifuge tests simplified the flexible barrier system and do not allow cable/anchor failure, a typical 22 mm diameter steel cable with 350 kN tensile strength is adopted here as a reference to check the degree of utilization of flexible barrier cable. It is found that the 20%-solid-fraction impact is characterized with the highest degree of utilization (85%) and dry debris impact the lowest (44%). None of the cable load reaches the tensile strength of the cable.

With the measured cable axial force and cable displacement, the data points could be further plotted in the force - displacement space (*e.g.*, lower intermediate cable, Fig. 3c). The area below represents the energy dissipated by the flexible barrier. This study provides a directly estimation of the energy dissipated by flexible barrier itself during the debris – barrier interaction process.

3.2. Momentum flux and impact force

The deduced free-flow depth and velocity time histories (Figs. 4a-7a) from the high-speed imagery form the basis of comparison between the mometum flux and the measured normal impact force on rigid and flexible barriers. The two-phase flows and dry debris avalanche are all characterized with maximum depth of about 1.0 m. Yet the peak velocity of dry debris avalanche (11.8 m/s) is much lower than that of the two-phase flow (18.4 m/s for 20%-solid-fraction flow). The strong solid-fluid interaction in low solid flows, more specifically the buffering effect of fluid phase, impedes the contact between solid grains, resulting in higher efficieny on conversion from gravitational potential to kinetic energy. More notably, the velocity and depth of two-phase flows reach their peak synchronously (Figs. 4a-6a), confirming a blunt snout of debris flows (Iverson, 1997). Whereas depth of dry debris avalanche peaks at the decreasing stage of flow veolocity (Fig. 7a), reflecting a tapered flow front (Ashwood and Hungr, 2016). As a product of velocity and depth, the momentum flux $\rho v^2 hw$ of dry debris avalanche (Fig. 7b) is only about 1/3 that of 50%-solid-fraction flow (Fig. 6b).

In order to deduce the impact force acting on the flexible barrier, a circular-curve mathematical representation is found to be a better approximation of a deformed cable under uniform debris impact pressure (Sasiharan et al., 2006). The measured cable force can be decomposed into a component normal to the barrier face and a component tangential to the barrier face. The normal components on the right and left sides of a flexible barrier cable counterbalance the impact force by the flow (Song et al., 2018b). From the conservation of momentum, the momentum per unit time (flux) forwarded onto the barrier equals to the

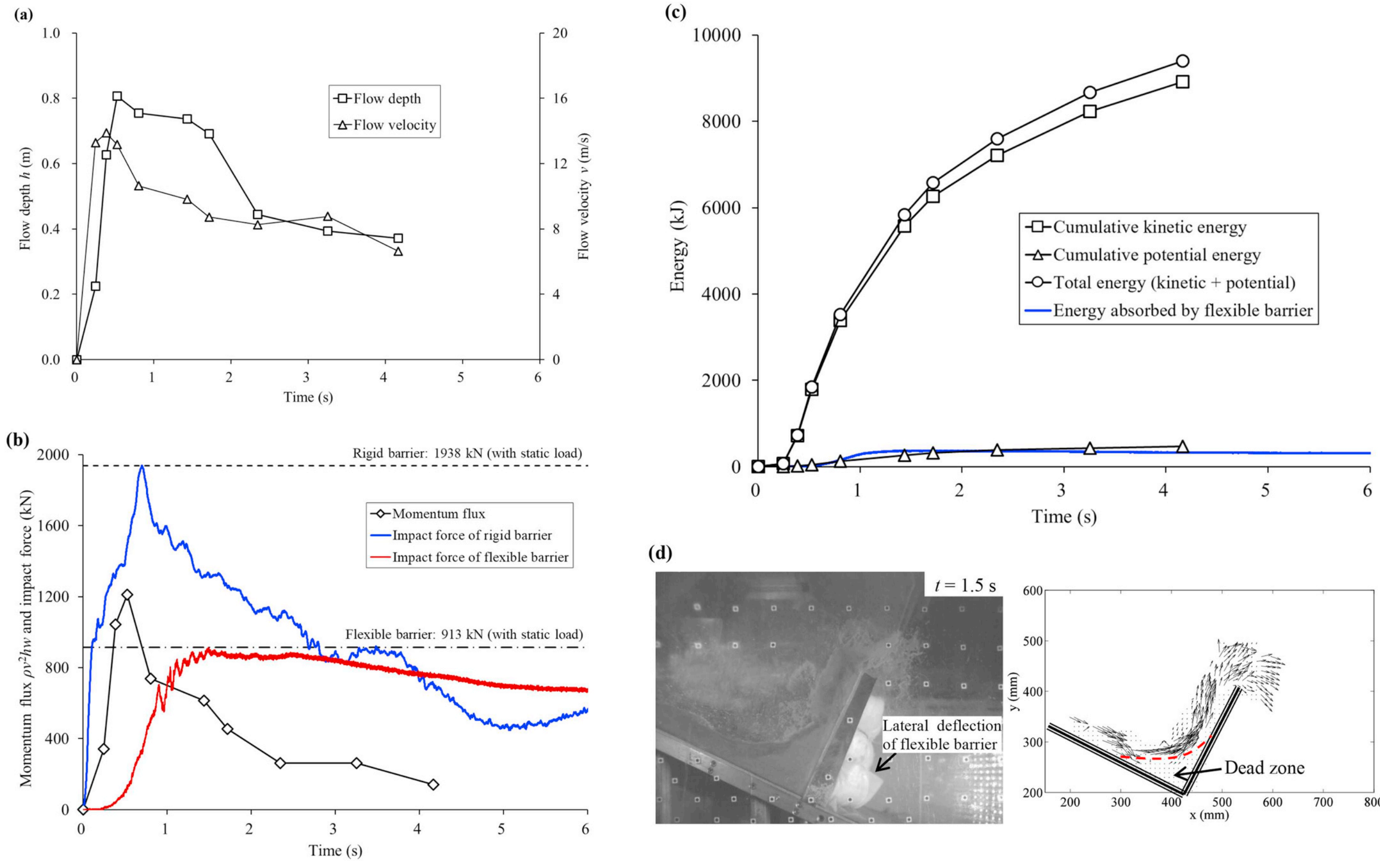

Fig. 5. Time histories of debris flow with 20% solid fraction (a) flow depth and velocity; (b) momentum flux and impact force; (c) debris energy and energy stored by flexible barrier; and (d) observed static load (dead zone revealed by PIV analysis) at the time instant when maximum energy is stored by flexible barrier.

resisting force exerted by the barrier. However, estimation of impact load without consideration of debris-structure interaction may not be conservative (Koo et al., 2017; Utili et al., 2015). The comparison of momentum flux and measured peak impact force implies that the momentum flux is not at all merely a surrogate of the impact force (Figs. 4b-7b; Table 3). Despite the significant lateral movement of flexible barrier (up to 33% of cable length, denoted as effect of barrier stiffness in Fig. 4b), impact load on flexible barrier (1228 kN) could still be higher than the momentum flux. Right after the flow front reaching the barrier, a static dead zone forms behind the barrier (see PIV result in Fig. 4d-7d). Thus the built-up of static load occurs simultaneously with the grow-up of impact force (Fig. 4b; Gao et al., 2017). The measured impact force is a combination of both dynamic (momentum flux) and static loads. In view of the significance to engineering design, further investigation on how the dead zone forms during the impact process, more specifically the contribution of static load to the peak force at different solid fractions, is warranted.

3.3. Energy dissipation by flexible and rigid barriers

Through the calibration tests, the cumulative debris flow kinetic energy passing through the section where barriers would be installed can be deduced from the flow depth and flow velocity ($\Sigma_0^t 0.5(\rho hwv\Delta t) v^2$; Figs. 4c-7c). By setting the barrier base as the datum line, the cumulative potential energy can be deduced ($\Sigma_0^t 0.5(\rho hwv\Delta t)gh \cos 25^{\circ}$, where 25° is the slope inclination, Figs. 4c-7c). Comparison between kinetic energy and potential energy denotes that the flows are all inertial-dominated (characterized with Froude number higher than unity). Through the reliable measurements on the cable elongation (Fig. 3a) simultaneously with the cable force (Fig. 3b), the work done by the flexible barrier can be deduced (Figs. 4c to 7c). Therefore, the proportion of energy dissipated by the flexible barrier to the total energy (kinetic + potential energy) could be systematically estimated. Regardless of the debris properties, the proportion of energy dissipated by the flexible barrier to total energy remains a surprisingly low level, ranging from 4.0–6.7% (Table 3), with an average of 5.6%. Since the kinetic energy is much higher than the potential energy, the proportion of energy dissipated by the flexible barrier to kinetic energy is close to that of total energy (Table 3). This denotes the distinct mechanisms in energy dissipation for rockfall and debris flow impact. It is assumed that majority of the kinetic energy of single rock block would be absorbed by the barrier system, which forms the basis of the “energy approach” for design of debris-flow flexible barrier. In contrast, debris flow impact results in over 90% of the energy dissipated through the internal and boundary shearing process (Ng et al., 2016b). In other word, the flexible barrier's capacity is not fully utilized if the rated energy capacity of a flexible barrier is adopted to resist debris flow.

The ratios of energy dissipated by the flexible barrier itself to the

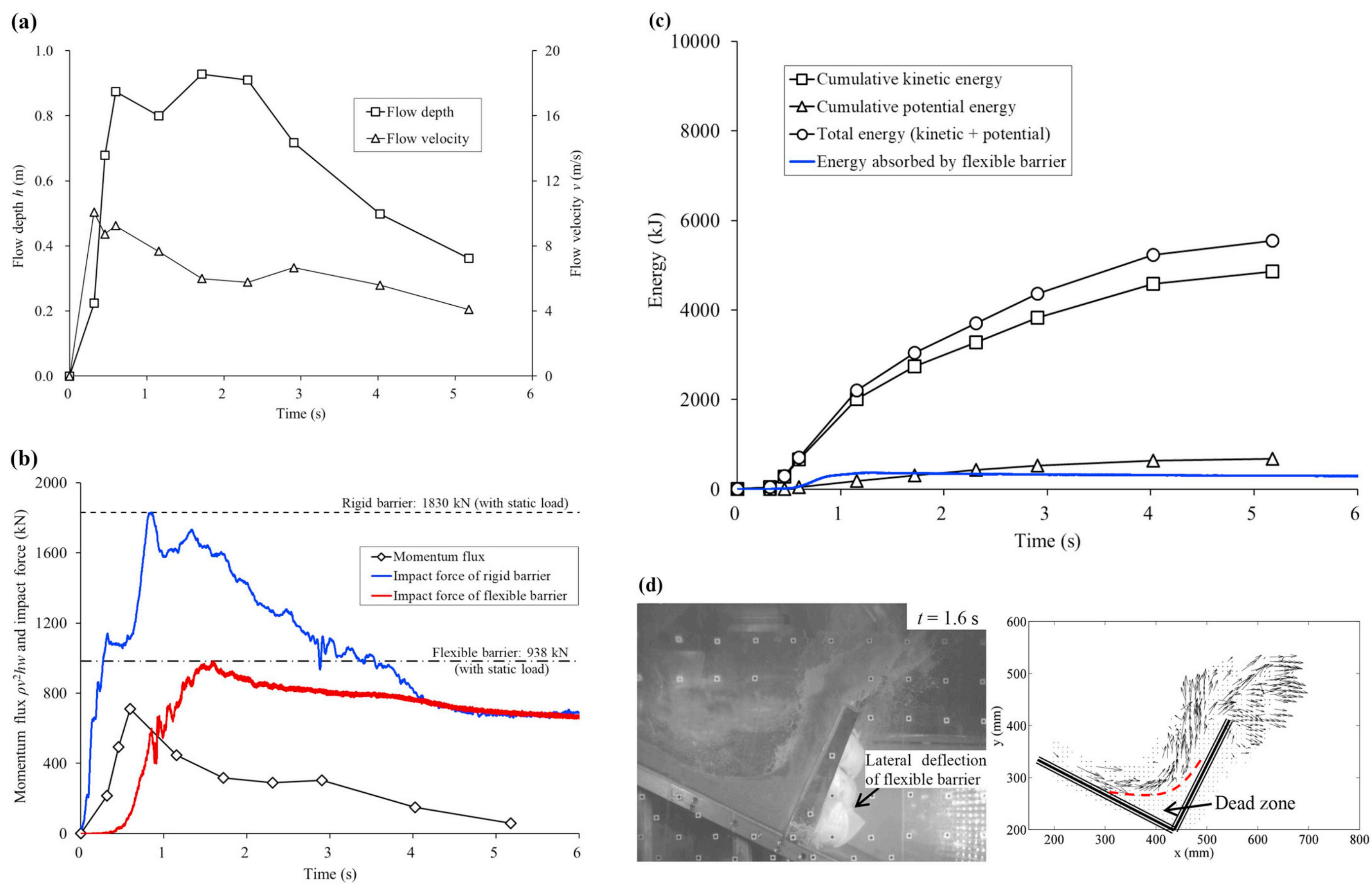

Fig. 6. Time histories of debris flow with 50% solid fraction (a) flow depth and velocity; (b) momentum flux and impact force; (c) debris energy and energy stored by flexible barrier; and (d) observed static load (dead zone revealed by PIV analysis) at the time instant when maximum energy is stored by flexible barrier.

total energy in this study (< 10%) substantially differ from that derived by Huo et al. (2017, 64%, physical modelling) and only match the lower limit derived by Cheung et al. (2018, 7% - 30%, numerical simulation). Yet it agrees well with the result of Kwan et al. (2018, 6%, numerical simulation). The ratios must be barrier-specific and related to the properties of debris flow. This further denotes the uncertainty of the "energy approach" in design of debris-flow flexible barriers. Except the steady state assumption made behind the calculation, two major aspects may contribute to this discrepancy: a) the influence of flow regime, *i.e.*, the degree of solid-fluid interaction; and b) geometrical factors, including the slope inclination and structural configuration of the flexible barriers. Further study should focus on these two aspects to shed light on the mitigation and energy dissipation mechanisms of flexible barriers.

One may postulate that the flexible barrier attenuates the impact load through the enhanced energy dissipation within the debris flow itself. Conceptually, the energy stored by a barrier $E = Fx/2 = F^2/2k$, where $F = kx$ is the impact force, k and x are the bulk stiffness and displacement, respectively. Thus, the energy absorbed by a barrier E is inversely proportional to the barrier stiffness k, denoting the negligible energy absorbed by the rigid barrier (Table 3, deduced using the measured bending moment in Fig. 2b and known bending stiffness) or even more energy dissipation within the debris flow. Yet the higher proportion of energy dissipated by flexible barrier does not invalidate that the flexible barrier facilitates a much milder debris-structure interaction (lower impact force) *via* a more efficient energy dissipation within the debris flow itself. From the momentum perspective, the impact attenuation is due to the prolonged interaction time with the flexible barrier. From the energy perspective, although with a higher proportion of energy absorbed than the rigid barrier, the attenuated peak force is due to the efficient mixing and shearing mobilized by the large barrier movement of flexible barrier.

3.4. Effects of debris-structure interaction

Different from the instantaneous concentrated load of rockfall impact (mechanism of extremely short duration), debris flows interact with barriers through a process that is rather continued over time (long-lasting interaction). As the flow body with distributed momentum and energy impacts the barrier, a dead zone forms at the barrier base (Fig. 4d-7d). Subsequent flow interacts with the static debris and then ramps up to the barrier face in a much milder manner, leaving majority of energy dissipated within the flow.

From the comparison between the energy stored by the flexible (rigid) barrier and the cumulative energy, it can be concluded that the debris-structure interaction plays a major role in the energy dissipation

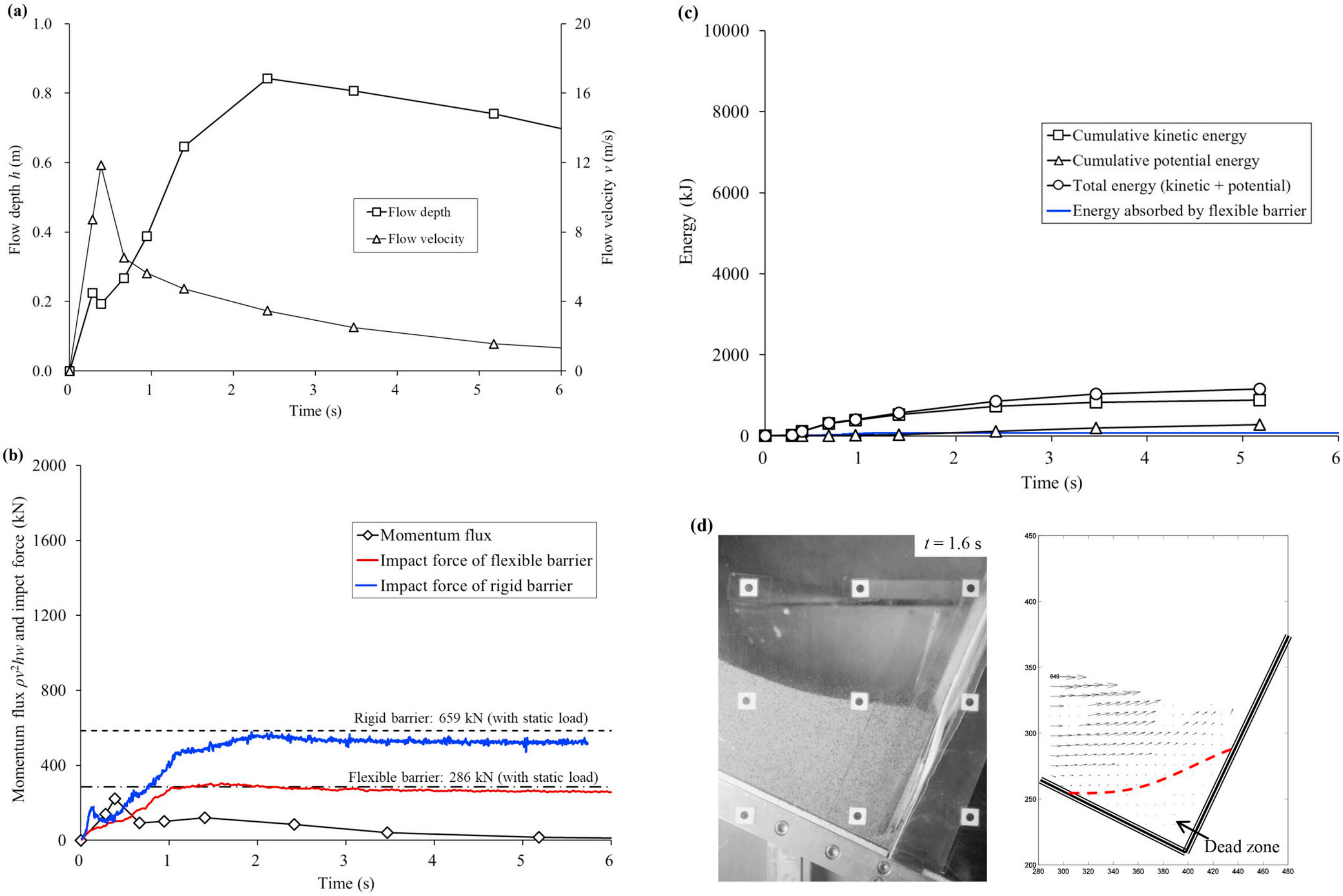

Fig. 7. Time histories of dry debris avalanche (a) flow depth and velocity; (b) momentum flux and impact force; (c) debris energy and energy stored by flexible barrier; and (d) observed static load (dead zone revealed by PIV analysis) at the time instant when maximum energy is stored by flexible barrier.

and impact load reconstruction. On one hand, through efficient mixing and internal shearing, it promotes a faster energy dissipation rate and thus the debris quickly approaches a static state. The enhancement in energy dissipation is a desired result for debris-resisting barrier design and this denotes that the current "energy approach" is on the conservative side for the design of debris-flow flexible barrier. One the other hand, the quick accumulation of static debris (dead zone) forms static load on the barrier, which is the main reason why the peak momentum flux cannot be directly adopted as the impact force.

4. Concluding remarks

An interpretation of debris flows impacting rigid and flexible barriers is presented in this study. For the first time in study of debris flow impacting flexible barrier, a quantitative analysis from the energy perspective has been conducted. Conclusions from this study can be drawn as follows:

(1) The difference between concentrated rockfall and distributed debris flow impact results in distinct energy dissipation ratio. While maintaining proper degree of utilization of the cable strength, a 1000 kJ flexible barrier could successfully intercept debris flows with total energy higher than the rated energy capacity of the barrier. In this study, majority portion (> 90%) of the total energy is actually dissipated in the process of internal and boundary shearing of debris flow itself.
(2) The "energy approach" cannot provide the internal structural forces and loads transferred to the flexible barrier foundation, which are necessary for the design of a flexible barrier system. However, the "energy approach" indeed is a pragmatic tool to evaluate the degree of debris-barrier interaction and to optimize the design of debris-flow flexible barrier.
(3) From the momentum perspective, with the contribution of the static debris, impact load could be higher than the momentum flux. Both the momentum and energy perspectives highlight the significance of considering debris-structure interaction for the design of debris flow resisting structures.

As a preliminary study of the debris-barrier interaction mechanism, only simplified debris materials and one specific barrier type were adopted. The amount of debris energy transferred to the flexible barrier actually depends on both the flow properties (*i.e.*, solid fraction, fluid viscosity, and flow regime) and structural properties of flexible barrier (*i.e.*, characteristics of energy-dissipating devices and overall stiffness of

Table 3
Momentum flux and proportion of kinetic energy absorbed by a 1000 kJ flexible barrier and a rigid barriers (all dimensions in prototype).

Solid fraction (%)	Density (kg/m^3)	Peak momentum flux (kN)	Peak force on rigid barrier (kN)	Peak force on flexible barrier (kN)	Kinetic energy (kJ)	Potential energy (kJ)	Total energy (kJ)	Energy stored by flexible barrier (kJ)	Ratio of stored to kinetic energy for flexible barrier (%)	Ratio of stored to total energy for flexible barrier (%)	Energy stored by rigid barrier (kJ)	Ratio of stored to total energy for rigid barrier (%)
20	1330	1190	1662	1228	7364	382	7746	400	5.4	5.2	0.0023	3.0E-05
40	1660	1212	1938	913	8921	476	9397	372	4.2	4.0	0.0036	3.8E-05
50	1825	710	1830	983	4857	686	5543	372	7.7	6.7	0.0035	6.3E-05
Dry	1530	259	659	286	881	276	1157	74	8.4	6.4	0.0001	8.6E-06

barrier). Further study on these two aspects are necessary to optimize the efficiency of debris-flow flexible barrier.

Acknowledgements

The authors acknowledge the financial support from the National Natural Science Foundation of China, China (grant No. 51809261, 5170091039, 11672318, and 11602284) and the CAS "Light of West China" Program, China (grant No. Y6R2220220). The authors are grateful for the financial support from research grant T22-603/15-N provided by the Research Grants Council of the Government of Hong Kong SAR, China.

References

Ashwood, W., Hungr, O., 2016. Estimating the total resisting force in a flexible barrier impacted by a granular avalanche using physical and numerical modeling. Can. Geotech. J. 53 (10), 1700–1717.

Berger, C., McArdell, B.W., Schlunegger, F., 2011. Direct measurement of channel erosion by debris flows, Illgraben, Switzerland. J. Geophys. Res. 116 (F1).

Cheung, A.K., Yiu, J., Lam, H.W., Sze, E.H., 2018. Advanced numerical analysis of landslide debris mobility and barrier interaction. HKIE Transactions 25 (2), 76–89.

Cui, Y.F., Zhou, X.J., Guo, C.X., 2017. Experimental study on the moving characteristics of fine grains in wide grading unconsolidated soil under heavy rainfall. J. Mt. Sci. 14 (3), 417–431.

Duffy, J.D., DeNatale, J.S., 1996. Debris flow mitigation using flexible Barriers. In: Proceedings of the 47th Annual Highway Geology Symposium, pp. 243–252.

Gao, L., Zhang, L.M., Chen, H.X., 2017. Two-dimensional simulation of debris flow impact pressures on buildings. Eng. Geol. 226, 236–244.

Huo, M., Zhou, J.W., Yang, X.G., Zhou, H.W., 2017. Effects of a flexible net barrier on the dynamic behaviours and interception of debris flows in mountainous areas. J. Mt. Sci. 14 (10), 1903–1918.

Iverson, R.M., 1997. The physics of debris flows. Rev. Geophys. 35 (3), 245–296.

Iverson, R.M., 2015. Scaling and design of landslide and debris-flow experiments. Geomorphology 244, 9–20.

Iverson, R.M., Logan, M., Denlinger, R.P., 2004. Granular avalanches across irregular three-dimensional terrain: 2. Experimental tests. J. Geophys. Res.: Earth Surf. 109 (F1).

Koo, R.C.H., Kwan, J.S.H., Ng, C.W.W., Lam, C., Choi, C.E., Song, D., Pun, W.K., 2017. Velocity attenuation of debris flows and a new momentum-based load model for rigid barriers. Landslides 14 (2), 617–629.

Kwan, J.S.H., 2012. Supplementary technical guidance on design of rigid debris-resisting barriers. In: GEO Report No. 270. Geotechnical Engineering Office, HKSAR Government.

Kwan, J.S.H., Cheung, R.W.M., 2012. Suggestion on design approaches for flexible debris-resisting barriers. In: Discussion note DN1/2012. Geotechnical Engineering Office, HKSAR Government.

Kwan, J.S.H., Chan, S.L., Cheuk, J.C.Y., Koo, R.C.H., 2014. A case study on an open hillside landslide impacting on a flexible rockfall barrier at Jordan Valley, Hong Kong. Landslides 11 (6), 1037–1050.

Kwan, J.S., Sze, E.H.Y., Lam, C., 2018. Finite element analysis for rockfall and debris flow mitigation works. Can. Geotech. J. https://doi.org/10.1139/cgj-2017-0628.

Ng, C.W.W., Song, D., Choi, C.E., Koo, R.C.H., Kwan, J.S.H., 2016a. A novel flexible barrier for landslide impact in centrifuge. Géotech. Lett. 6, 221–225.

Ng, C.W.W., Song, D., Choi, C.E., Liu, L.H.D., Kwan, J.S.H., Koo, R.C.H., Pun, W.K., 2016b. Impact mechanisms of granular and viscous flows on rigid and flexible barriers. Can. Geotech. J. 54 (2), 188–206.

Sasiharan, N., Muhunthan, B., Badger, T.C., Shu, S., Carradine, D.M., 2006. Numerical analysis of the performance of wire mesh and cable net rockfall protection systems. Eng. Geol. 88 (1), 121–132.

Schofield, A.N., 1980. Cambridge geotechnical centrifuge operations. Geotechnique 30 (3), 227–268.

Song, D., Ng, C.W.W., Choi, C.E., Zhou, G.G.D., Kwan, J.S.H., Koo, R.C.H., 2017. Influence of debris flow solid fraction on rigid barrier impact. Can. Geotech. J. 54 (10), 1421–1434.

Song, D., Choi, C.E., Zhou, G.G.D., Kwan, J.S.H., Sze, H.Y., 2018a. Impulse load characteristics of bouldery debris flow impact. Géotech. Lett. 8 (2), 111–117.

Song, D., Choi, C.E., Ng, C.W.W., Zhou, G.G.D., 2018b. Geophysical flows impacting a flexible barrier: effects of solid-fluid interaction. Landslides 15 (1), 99–110.

Sun, H.W., Law, R.P.H., 2015. A preliminary study on impact of landslide debris on flexible barriers. In: GEO Report No. 309. Geotechnical Engineering Office, HKSAR Government.

Utili, S., Zhao, T., Houlsby, G.T., 2015. 3D DEM investigation of granular column collapse: evaluation of debris motion and its destructive power. Eng. Geol. 186, 3–16.

Volkwein, A., 2014. Flexible debris flow barriers. design and application. In: WSL Berichte, 18. Birmensdorf, Swiss Federal Institute for Forest, Snow and Landscape Research WSL (29 p).

Wei, Z.L., Shang, Y.Q., Lü, Q., Yu, Z., Pan, P., 2017. Application and design of an efficient siphon dewatering system for debris flow mitigation: a case study of a small catchment in Zhejiang Province, China. Eng. Geol. 226, 146–160.
Wendeler, C., 2008. Murgangrückhalt in Wildbächen - Grundlagen zu Planung und Berechnung von flexiblen Barrieren. In: Diss. ETH Nr. 17916.
Wendeler, C., Volkwein, A., Denk, M., Roth, A., Wartmann, S., 2007. Field measurements used for numerical modelling of flexible debris flow barriers. In: Chen, C.L., Major, J.J. (Eds.), Proceedings of Fourth International Conference on Debris Flow Hazards Mitigation: Mechanics, Prediction, and Assessment, Chengdu, China, 10–13 September. Vol. 2007. pp. 681–687.
Wendeler, C., Volkwein, A., McArdell, B.W., Bartelt, P., 2018. Load model for designing flexible steel barriers for debris flow mitigation. Can. Geotech. J. https://doi.org/10.1139/cgj-2016-0157.
WSL, 2009. Full-scale testing and dimensioning of flexible debris flow barriers. In: Technical report 1–22. WSL, Birmensdorf.
WSL, 2011. Report on testing SL-150 a protection system against shallow landslides. In: Test Report No. 10-17. WSL, Switzerland.
Zhang, S., 1993. A comprehensive approach to the observation and prevention of debris flows in China. Nat. Hazards 7 (1), 1–23.